Applied Physics Letters

Dielectric barrier discharge induced boundary layer suction

Cite as: Appl. Phys. Lett. **100**, 264103 (2012); https://doi.org/10.1063/1.4731288
Submitted: 13 March 2012 . Accepted: 12 June 2012 . Published Online: 27 June 2012

S. Im, and M. A. Cappelli

Dielectric barrier discharge induced boundary layer suction

S. Im and M. A. Cappelli
Mechanical Engineering Department, Stanford University, Stanford, California 94305-3032, USA

(Received 13 March 2012; accepted 12 June 2012; published online 27 June 2012)

Boundary layer downdraft suction and through-surface fluid removal is demonstrated with a streamwise oriented dielectric barrier discharges fabricated into a flat plate immersed in a 3.8 m/s freestream flow (Re = 72000). The velocity field is obtained by particle image velocimetry. Suction with through-surface fluid removal is found to thin the boundary layer and increases the velocity gradient in the vicinity of the wall by extracting slower fluid from the inner layer region. The effect of this suction on the boundary layer persists away from the center of the exposed electrode without inducing significant disturbances to the freestream flow. © *2012 American Institute of Physics*. [http://dx.doi.org/10.1063/1.4731288]

Boundary layer suction is one of several methods used to control boundary layer flows.[1] The principle of boundary layer suction is that the low speed fluid in a viscous fluid layer near a surface is drawn through the surface of an aerodynamic body upstream of an adverse pressure gradient. It has been studied for over a century because of its practical advantages in aerodynamics to control flow separation,[2,3] drag reduction,[4,5] and to suppress or re-laminarize boundary layer turbulence.[6] In lifting bodies, suction can lead to a reduction in drag and to an increase in lift. Despite this rich history, turbulent boundary layer control by boundary layer suction is still an active field of research. In its usual application, boundary layer suction requires a pumping device, adding significant weight and complexity to the airframe. A boundary layer suction mechanism free of moving mechanical parts can greatly simplify its implementation. In this paper, we describe such an approach using model-integrated dielectric barrier plasma discharges for local flow forcing.

There have been several studies of flow control through the use of surface-mounted dielectric barrier discharge (DBD) actuators since first introduced as a means of aerodynamic forcing by Roth *et al.*[7] A typical DBD consists of flow-exposed and dielectric embedded electrodes driven by alternating current (AC) designed to impose a force on the ionized gas generated by the discharge and to induce a directional flow of neutral gas through collisions with the drifting ions. This induced directional flow can be quite effective in boundary layer re-attachment,[8–10] boundary layer transition delay,[11] and turbulent boundary layer control in both subsonic[12] and supersonic[13] flow regimes. To compliment these experimental studies, robust models and simulations of actuator performance have also been developed.[14] However, there has been no demonstration in which DBD actuators have been used to generate downward flow in conjunction with the removal of low-speed surface-adjacent fluid from the flow. In flow applications, this bleeding is important in minimizing the formation of secondary flows in the boundary layer region. In this letter, we describe studies in which barrier discharges are used in such a configuration for turbulent boundary layer thinning.

The experiment consists of DBD actuators fabricated into a flat plate model and with particle image velocimetry (PIV) used to characterize the velocity fields. A 20° leading edge wedged acrylic flat plate (5 mm thick, 130 mm wide, and 230 mm long) is positioned in the center of a w = 300 × H = 300 mm cross sectional area vertical wind tunnel that can produce a 3.8 m/s freestream flow ($Re_w = 72000$). A symmetric DBD actuator pair is integrated into the top surface of the flat plate as illustrated in the top view of Fig. 1(a) and cross sectional view of Fig. 1(b). The exposed electrode is a single copper strip, oriented parallel to the base flow. These electrodes (exposed and embedded, each 0.1 mm thick) are 135 mm in length and 7 mm wide and 135 mm in length and 50 mm wide, respectively. The exposed electrode is centered over the buried electrode, and both electrodes are placed along the center of the model 50 mm downstream from the leading edge. Kapton tape (50 μm thick) and an acrylic plate are used as a dielectric layer to isolate the embedded electrode. Sand paper (120 Grit, 130 mm wide, and 20 mm long) is attached to the top of the flat plate 5 mm downstream from the leading edge to serve as a turbulent trip, creating a turbulent boundary layer flow. Two parallel suction slots (1.5 mm wide) straddle the exposed electrode, 1 mm from either side (i.e. 5 mm from center of flat plate). These slots lead to a 2 mm high inner channel which carries away the drawn fluid eventually bleeding this fluid into the freestream, as shown in Fig. 1(b). Two additional asymmetric DBD actuator pairs are built into the inner (upper) surface of this channel to further drive this internal flow. The exposed electrodes in each of these additional actuator pairs are located 35 mm from the center of the flat plate while the embedded electrodes, encapsulated with Kapton tape, are placed 42 mm from the center of the flat plate. Both exposed and embedded electrodes are 7 mm wide and 115 mm in length. Cast acrylic (1.5 mm thick) and Kapton tape (50 μm thick) are used as the dielectric barrier for these internal asymmetric actuators. In this configuration, the main electrode pair serves to produce a symmetric spanwise forcing producing a downward flow (see Fig. 1(b)) leading to a displacement of the boundary layer flow by the higher speed fluid. A portion of the slower boundary layer fluid is swallowed by the adjacent slots and driven laterally within the internal channel by the asymmetric actuators creating a forced internal flow, in much the same way that a pump

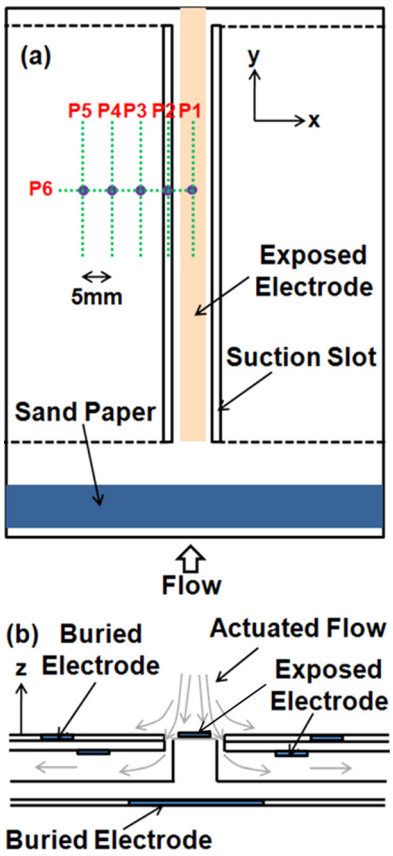

FIG. 1. (a) Top view and (b) cross-sectional view of the DBD suction device.

serves to drive a suction flow in a more conventional boundary-layer bleed system.

Two independent AC power supplies are used to power the dielectric barrier discharges. The main symmetric actuator is driven by a Minipuls 6 power supply. In this study, the operating voltage and frequency are 14.5 kV (peak-to peak) and 15 kHz, respectively. The power consumption of the primary electrode pair is 14 W. The two asymmetric actuators are powered by an Information Unlimited PVM 300 generator with a driving voltage and frequency of 12 kV (peak-to peak) and 25 kHz, respectively. The combined power used by the internal electrode pairs is 15 W.

A Nd:YAG laser (New wave, Gemini PIV, 100 mJ/pulse energy, 10 Hz, 532 nm) is shaped into a thin sheet (300 μm thick) using two cylindrical and one convex spherical lenses and is directed into the test section for the PIV studies. The scattering from five 2D imaging planes (P1 to P5) separated by 5 mm are recorded, starting from the center line of the flat plate (referred as plane 1, P1), and stereo PIV is performed at the plane (P6) which is perpendicular to the five 2D planes, as depicted in Fig. 1(a). In addition to the resulting velocity field, the images from P1 and P5 are used to construct velocity profiles at a location 135 mm from the leading edge. Without flow actuation, the boundary layer thickness in this region is about 9 mm giving rise to a local Reynolds number (based on this boundary layer thickness) of $\mathrm{Re}_\delta = 2180$. In carrying out the PIV studies, double exposure CCD cameras (LaVision, Imager Intense) capture the scattered light from the seeded aluminum oxide particles. The velocity vector field is obtained from two instantaneous

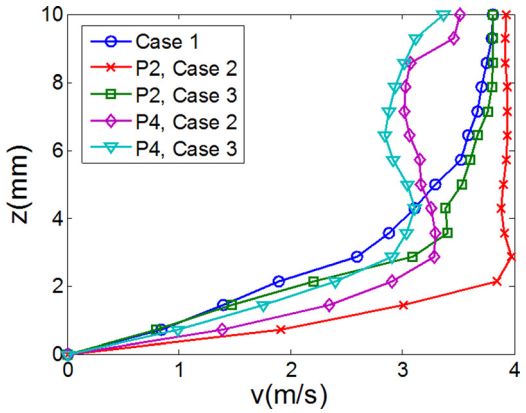

FIG. 2. Mean streamwise velocity profile at the P2 and P4 imaging planes 135 mm from the leading edge.

sequential images taken with a 50 μs time delay. Laser shot timing and the triggering of the camera are synchronized by DaVis 7 software. PIV images are taken with three different flow conditions: (Case 1) flow without actuation, (Case 2) flow with actuation (i.e., all DBD actuators active and open suction slots), and (Case 3) flow with actuation by the exterior DBD but with the suction channel asymmetric DBD actuators inactivated and all slots blocked. A comparison of Case 2 and Case 3 would highlight the role of DBD-induced boundary layer bleeding which is the main contribution of this work.

The mean streamwise component velocity profiles at 135 mm from the leading edge for Cases 1–3 at the P2 and P4 imaging regions (obtained by ensemble averaging 100 instantaneous PIV images) are shown in Fig. 2. It is apparent from the P2 plane data that DBD actuation draws a higher momentum flow from the freestream into the boundary layer in the vicinity of the exposed electrode by comparing Case 1 (blue circles) to Case 2 (red crosses). As a result, the boundary layer is thinned from $\delta_{\mathrm{Case1}} \sim 9$ mm to $\delta_{\mathrm{Case2}} \sim 2$ mm and the momentum thickness is reduced from $\theta_{\mathrm{Case1}} \sim 1.09$ mm to $\theta_{\mathrm{Case2}} \sim 0.32$ mm. Boundary layer thinning is more dramatic in Case 2 compared to Case 3 (green squares) where only the external flow actuator is active and the bleed channel actuators are inactive and the channels are blocked. Case 3 results in a momentum thickness of $\theta_{\mathrm{Case3}} \sim 0.83$ mm a boundary layer thickness $\delta_{\mathrm{Case3}} \sim 8$ mm. A similar but correspondingly weaker flow response is observed in the P4 plane located 10 mm away from the suction slot. Again, the DBD actuation of Case 2 (purple diamonds) draws higher momentum flow to the vicinity of the wall as seen when comparing to Case 1. However, the effect of this actuation is not as strong as that seen in the plane P2 closer to the slot. The result for Case 3 (light blue inverted triangle) indicates that operation with the internal suction flow DBD results in some (but little) benefit at this plane. The reduced velocity at larger distances from the surface suggests the presence of secondary flows.

The mean streamwise velocity profiles for the base flow and activated flow along the 135 mm from the leading edge for Case 2 (also extracted from ensemble averaged 100 instantaneous PIV images) from P1 to P5 are compared in Fig. 3. Because of the symmetry of the external flow actuator,

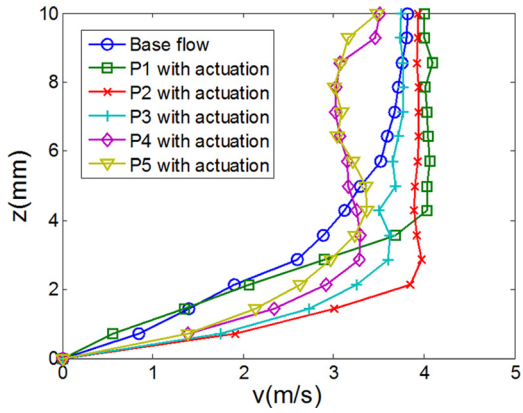

FIG. 3. Mean streamwise velocity profiles 135 mm from the leading edge (Case 1 and Case 2).

P1 is as a stagnation plane with the actuated flow shown schematically in Fig. 1(b). Actuation does thin the boundary layer in this plane but depicts a similar slope to the inactivated Case 1 flow close to the wall. The most noticeable effect of actuation is seen in regions of the flow displaced slightly in the spanwise direction from the stagnation plane, i.e., in the planes designated P2 and P3; planes that are in close proximity to the suction slot. The thickness of boundary layer is reduced dramatically as a result of the actuation and suction, and the slope of boundary layer profile is steepened significantly in the near wall region. This steepening comes at the expense of the momentum in the outer region of the boundary layer. Further from the stagnation plane, we see, by examining the flow in the P4–P5 planes, that while the near wall boundary layer profile remains steep the distant boundary suffers severe degradation indicative of the presence of a more complex three dimensional flow.

Velocity fields for Cases 1–3 for the image region P6 (acquired by ensemble averaged 100 stereo PIV image pairs) are shown in Figs. 4(a)–4(c), respectively. We note that the direction of the freestream flow in these images is out of the page. The freestream flow component (y-direction) is depicted by the color scheme (red is high, blue is low) while the other two components are represented by arrows. It is seen in Fig. 4(a) that there is slight thinning of the boundary layer in the vicinity of the slot even when plasma actuators are not activated. We believe that this is caused by a pressure difference between the slot and the suction channel exit due to a non-uniform flow around the entire body. However, this effect is minor in comparison to Case 2, as seen in Fig. 4(b), which thins the boundary layer by approximately 80% (boundary layer thickness reduced from 9 mm to 2 mm). With the Case 2 flow (Fig. 4(b)) there is strong flow in the vicinity of the slot, more so when the slot is open than when it is blocked (Case 3), as seen in Fig. 4(c). The evidence that there is less disturbance to the freestream flow in Case 2 than in Case 3 can be found in Figs. 5(a) and 5(b), which depict vorticity contour fields in the P6 plane for Cases 2 and 3, respectively. The location of the vortex induced by actuation in Fig. 5(a) is closer to the wall than in Fig. 5(b). In addition, Case 2 has less of a secondary flow region while Case 3 has a strong x-directional component to the flow further from the electrodes.

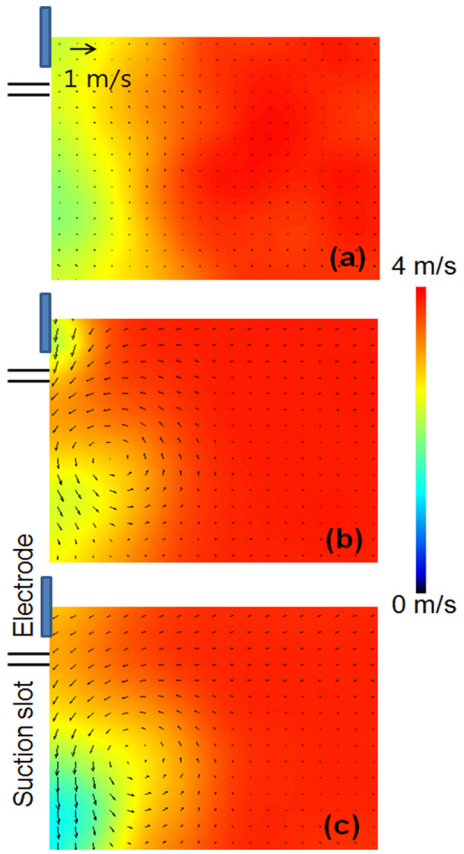

FIG. 4. Mean 3D flow field for the P6 plane (a) without actuation (Case 1), (b) plasma actuation with suction (Case 2), (c) plasma actuation without suction (Case 3, i.e., internal channel DBD inactive and slots are blocked).

In this letter, we demonstrate that a dielectric barrier discharge can provide a means of controlling boundary layers via suction. An external-flow symmetric and two internal asymmetric DBD actuators are fabricated into an acrylic flat plate designed to ingest and redirect boundary layer flow through a suction slot and bleed channel. In this scheme, the DBD actuators accomplish this suction and boundary layer bleed with no moving parts. Measurements are made in a wind tunnel operated 3.8 m/s freestream flow ($Re_w = 72000$), and PIV is used to capture the velocity field in regions close to the induced stagnation plane. It is found that the boundary layer thickness can be reduced by suction-induced actuation and velocity gradients at the vicinity of the wall can be increased, leading to increased resistance to separation. The influence of this actuation persists as far as ten times the suction slot width (~15 mm) along a spanwise direction from the suction slot,

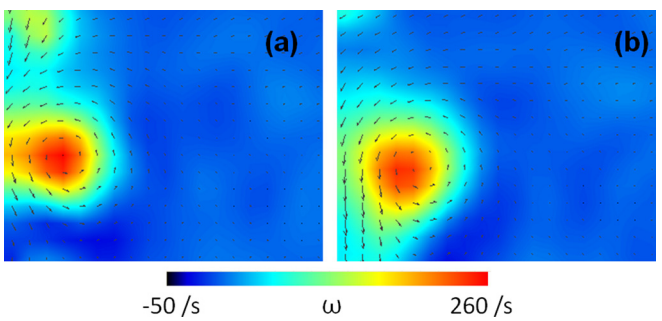

FIG. 5. Vorticity contour for the P6 plane (a) plasma actuation with suction (Case 2), (b) plasma actuation without suction (Case 3).

which, like the discharge actuators, is aligned in the streamwise direction without generating significant flow disturbances to adjacent fluid. Secondary flows generated by the DBD actuation are also characterized by PIV and the secondary flows appear to be reduced considerably when the all electrodes are activated with open suction slots.

This work is sponsored by the Predictive Science Academic Alliance Program (PSAAP) at Stanford University, funded through the Department of Energy.

[1]H. Schlichting, *Boundary Layer Theory* (Mcgraw-Hill, New York, 1965).
[2]M. Sano and N. Hirayama, Bull. JSME **28**, 807 (1985).
[3]S. A. Gbadebo, B. A. Cumpsty, and T. P. Hynes, J. Turbomach. **130**, 011004 (2008).
[4]R. A. Antonia, Y. Zhu, and M. Sokolov, Phys. Fluids. **7**, 2465 (1995).
[5]J. Park and H. Choi, Phys. Fluids **11**, 3095 (1999).
[6]M. A. Badrinarayanan, J. Fluids Mech. **31**, 609 (1968).
[7]J. R. Roth, D. M. Sherman, and S. P. Wilkinson, "Boundary Layer Flow Control with a One Atmosphere Uniform Glow Discharge Surface Plasma," *36th AIAA Sciences Meeting and Exhibit*, AIAA Paper No. 1998-0328, 1998.
[8]M. L. Post and T. C. Corke, AIAA J. **42**, 2177 (2004).
[9]Y. Sung, W. Kim, M. G. Mungal, and M. A. Cappelli, Exp. Fluids **41**, 479 (2006).
[10]H. Do, W. Kim, M. G. Mungal, and M. A. Cappelli, "Bluff Body Flow Separation Control using Surface Dielectric Barrier Discharges," *45th AIAA Aerospace Sciences Meeting and Exhibit*, AIAA Paper No. 2007-939, 2007.
[11]S. Grundmann and C. Tropea, Exp. Fluids **42**, 653 (2007).
[12]C. O. Porter, J. W. Baughn, T. E. McLaughlin, C. L. Enloe, and G. I. Font, AIAA J. **45**, 1562 (2007).
[13]S. Im, H. Do, and M. A. Cappelli, Appl. Phys. Lett. **97**, 041503 (2010).
[14]E. Moreau, J. Phys. D **40**, 605 (2007).